Latin American Journal of Solids and Structures
www.lajss.org

Elastoplastic Stability and Failure Analysis of FGM Plate with Temperature Dependent Material Properties under Thermomechanical Loading

Abstract

The present paper explores the stability and failure response of elastoplastic Ni/Al_2O_3 functionally graded plate under thermomechanical load using non-linear finite element formulation based on first-order shear deformation theory and von-Karman's nonlinear kinematics. The temperature dependent thermoelastic material properties of FGM plate are varied in the thickness direction by controlling the volume fraction of the constituent materials (i.e., ceramic and metal) with a power law, and Mori-Tanaka homogenization scheme is applied to evaluate the properties at a particular thickness coordinate of FGM plate. The elastoplastic behavior of FGM plate is assumed to follow J_2-plasticity with isotropic hardening, wherein the ceramic phase is considered to be elastic whereas the metal is assumed to be elastic-plastic in accordance with the Tamura-Tomota-Ozawa model. Numerical studies are conducted to examine the effects of material and geometrical parameters, viz. material in-homogeneity, slenderness and aspect ratios on the elastoplastic bucking and postbuckling behavior and the failure response of FGM plate. It is revealed that material gradation affects the stability and failure behavior of FGM plate considerably. Furthermore, it is also concluded that FGM plate with elastic material properties exhibits only stable equilibrium path, whereas the elastoplastic FGM plate shows destabilizing response after the ultimate failure point.

Keywords

Functionally graded material (FGM); Elastoplastic analysis of FGM; Failure and stability of FGM plate; Nonlinear finite element method.

Kanishk Sharma [a]
Dinesh Kumar [b]

[a] Mechanical Engineering Department, Malaviya National Institute of Technology, Jaipur, 302 017, India, kanishksharma2009@gmail.com
[b] Mechanical Engineering Department, Malaviya National Institute of Technology, Jaipur, 302 017, India, dkumar.mech@mnit.ac.in

http://dx.doi.org/10.1590/1679-78253747

Received 06.02.2017
In revised form 12.05.2017
Accepted 16.05.2017
Available online 26.05.2017

1 INTRODUCTION

After a long use of isotropic and homogeneous materials such as steel, aluminium etc. for various engineering structures over the centuries, composite materials have found many applications since 1940's, not only for engineering structures but for all other engineering applications, because of their high specific strength and stiffness. During last decades, a new kind and advanced form of composite material, called functionally graded material (FGM), developed initially by a group of scientists in Japan as a thermal barrier material under extremely high temperature conditions for aerospace structures and fusion reactors, has found increasing applications in numerous engineering fields. FGM is an advanced, inhomogeneous composite material made by continuously varying its properties, in any predefined (usually along thickness) direction(s), by altering the volume fractions of the constituent materials (usually ceramic and metal). Continuous variation of properties would effectively avoid stress concentration seen in traditional laminate or fiber-reinforced composites. The better thermal characteristics of the ceramic constituent make these FGMs to withstand high-temperature environments, while the metal constituent provides the required mechanical strength against catastrophic fracture (Reddy, 2000; Reddy and Chin, 1998; Shiota and Miyamoto, 1997; Suresh and Mortensen, 1998).

Moreover, thin-walled structural elements in the forms of plates and shells, used extensively in various engineering applications, are more susceptible to buckling, large amplitude deflections, or excessive stresses under different in-plane mechanical and/or thermal loading (compression and/or shear) conditions. Efficient design of such thin plate-like structures requires utilization of postbuckling reserve strength beyond buckling (Arbocz and maggiori, 1987; Singh and Kumar, 1999). Therefore, being one of the major design criteria, it is important to study buckling and postbuckling characteristics of FGM plates/panels under mechanical, thermal or thermomechanical loading for their optimal, accurate and reliable design. There are numerous studies to-date on the vibration, buckling/stability analysis, and static and dynamic analysis of functionally graded (FG) plates and shells.

After the first attempt by Birman (1995) to solve the buckling problem of functionally graded hybrid composite plates under uni-axial compressive loading, numerous works have been devoted only to buckling analysis of FGM plates under various mechanical and/or thermal loads (Javaheri and Eslami, 2012; Lanhe, 2004; Matsunaga, 2009; Najafizadeh and Eslami, 2012; Samsam Shariat and Eslami, 2006). In addition, many researchers have also conducted various postbuckling analysis of FGM plates under thermal and/or mechanical loads. Liew et al. (2003) examined the postbuckling behavior of functionally graded rectangular plates integrated with surface-bonded piezoelectric actuators using the Reddy's higher-order shear deformation plate theory. Yang and Shen (2003) developed a semi-numerical approach using perturbation technique in conjunction with 1-D differential quadrature approximation and Galerkin procedure to study the large deflection and postbuckling responses of FGM rectangular plates under transverse and in-plane mechanical loads. An analytical solution to study the postbuckling behavior of moderately thick FGM plates and shallow shells under edge compressive loads and a temperature field was developed by Woo et al. (2005). Using 3-D finite element method, Na and Kim (2006) conducted 3-D thermal buckling and postbuckling analysis of FGM plates with temperature dependent material properties, subjected to uniform and non-uniform temperature rise. Shen (2007) presented the thermal postbuckling analysis of

a simply-supported, shear deformable FGM plates with temperature-dependent properties. The stability of simply-supported rectangular FGM plates with temperature dependent material properties, under in-plane thermomechanical loading was investigated by Duc and Tung (2010). Wu et al. (2007) predicted the postbuckling response of the alumina/aluminium FGM plate, subjected to thermal and mechanical loadings using fast converging finite double Chebyshev polynomials. Lee et al. (2010) investigated the postbuckling behavior of FGM ceramic-metal plates under edge compression and temperature field conditions using element free kp-Ritz method. The layer-wise finite element formulation for static and dynamic analysis of a FGM plate with surface-bonded piezoelectric layers was studied by Shakeri and Mirzaeifar (2009). Cinefra and Soave (2011) also used the layer-wise formulation to obtain the closed form solutions for free vibration problems of simply-supported FGM plates. Yaghoobi et al. (2015) investigated the thermal buckling analysis of hybrid laminated plates made of two-layered functionally graded materials (FGMs) integrated with surface-bonded piezoelectric actuators under uniform temperature rise and constant actuator voltage.

It is also well known that the structure's failure may be caused by material failure and/or instability. Further, before the material failure, the structure shows inelastic response which in turn causes a destabilizing effect on structures. Moreover, even for structures operating under elastic limit, safety concerns require the consideration of overloads that inevitably produce inelastic deformations (Bazant et al., 1993). Therefore, in practical scenario wherein the stresses induced in the structures by in-plane mechanical and/or thermal loads overpass the elastic limit of material, a suitable elastoplastic analysis is required for reliable, accurate and stable design of these structures under various loading conditions. Being an important design criterion, the elastoplastic buckling behavior of isotropic and composite plates have been analyzed by many researchers (see Bakker et al., 2009; Bi et al., 2014; Durban and Zuckerman, 1999; Paley and Aboudi, 1991; Soh et al., 2000). However, comparatively very few investigations have been made for inelastic buckling analysis of FGM structures. Fu et al. (2014) presented the elastoplastic buckling and post-buckling analysis of the functionally graded metal-metal sandwich plates with interfacial damage under mechanical loading conditions. The elastic-plastic stability analysis of FGM shells under various type of mechanical loading conditions was carried out by Huang et al. (2014) and Zhang et al. (2015) to derive the expressions for elastic and plastic critical buckling loads. Most of the relevant past studies have simplified the analysis by keeping the material properties unaffected by temperature, but such simplification does not hold good for FGM plate, intended to be used under high temperature conditions (Birman and Byrd, 2007). Further, there are no works on elastoplastic stability behavior of FGM plate under thermomechanical loading conditions, which is considered to be reasonable in the FGM under critical loading conditions because the ductility and good shear strength induced by the metal phase relax the stress concentration induced around the inherited cracks and flaws of ceramics through the plastic deformation (Bandyopadhyay et al., 2000; Soh et al., 2000). Moreover as the FGMs are intended to be used under critical temperature conditions, the possibility of plastic flow induced due to excessive heat flow is also inevitable.

Based on the aforementioned literature study, it is aimed in this paper to explore the elastoplastic buckling, postbuckling and failure analysis of FGM plate under thermomechanical conditions, with temperature dependent material properties. The actual non-homogeneous (along thickness) FGM plate with continuously varying properties along thickness is modelled as a laminate

composed of multiple perfectly-bonded layers of isotropic material having layer-wise constant composition (Sharma and Kumar, 2016a, 2016b). A non-linear FEM formulation based on the first-order shear deformation theory and the von-Karman's nonlinear kinematics is utilized. The elastoplastic behavior of FGM plate is assumed to follow J_2-plasticity and isotropic hardening in which the ceramic phase was considered to be elastic whereas the metal is taken to be elastoplastic material in accordance with the TTO model. Subsequently, a parametric study is conducted to investigate the effect of various parameters viz. nonlinear temperature dependence of material properties, material inhomogeneity (i.e., power exponent n), aspect ratios (i.e., a/b), slenderness ratios (i.e., b/h), and loading conditions on the elastoplastic buckling and postbuckling behavior, and the failure response of FGM plate under combined thermal and mechanical loading conditions.

2 EFFECTIVE THERMOELASTIC MATERIAL PROPERTIES OF FGM PLATE

A FGM plate, consisting of two constituents: ceramic (Al_2O_3) and metal (Ni), with a, b and h as its length, width and thickness, respectively is considered. The actual non-homogeneous FGM plate with continuously varying properties along thickness is modeled as a laminate composed of multiple perfectly-bonded layers of isotropic material having a layer-wise constant composition, as shown in Figure 1.

The volume fractions of ceramic and metallic constituents are assumed to follow, along the thickness of FGM plate, the power law distribution as follows:

$$V_m(z) = \left(\frac{z}{h} + \frac{1}{2}\right)^n ; V_c(z) = 1 - V_m(z) \tag{1}$$

where V denotes the volume fraction a constituent. The subscripts c and m, respectively, correspond to the ceramic and the metallic constituents. n is a variable called power law exponent, which determines the material variation profile along thickness coordinate z (varying in the range $-h/2 \leq z \leq h/2$).

As the potential applications of FGMs involve high-temperature conditions wherein, strong temperature dependence of material properties is expected. Hence it is necessary to consider temperature dependent material properties for accurate and reliable design of FGM structures. In the present study, the temperature-dependent thermal (i.e., thermal expansion coefficient α) and mechanical (i.e., Young's modulus E) properties of FGM plate are evaluated using below equation (Touloukian and Center, 1967).

$$P_j(T) = P_0(P_{-1}T^{-1} + 1 + P_1T + P_2T^2 + P_3T^3) \tag{2}$$

where $P(T)$ represents material property (E or α) evaluated at temperature T, and P_0, P_{-1}, P_1, P_2 and P_3 are the coefficients to calculate these temperature dependent material properties for Al_2O_3 and Ni. The values of these coefficients for Al_2O_3 and Ni are given in Table 1 (Reddy and Chin, 1998). The variation of these material properties for Al_2O_3 and Ni with temperature is shown in Figure 2.

The graded thermoelastic material properties across the thickness of FGM plate, at the mid of each layer in the case of layer-wise modeling of FGM plate used herein, are calculated using Mori-Tanaka scheme (Benveniste, 1987; Mori and Tanaka, 1973). According to the Mori–Tanaka homog-

enization method the effective bulk modulus $K(z,T)$, thermal expansion coefficient $\alpha(z,T)$ and the effective shear modulus $G(z,T)$ of the functionally graded material are calculated using following expressions:

$$\frac{\mathrm{K(z,T)-K_m(T)}}{\mathrm{K_c(T)-K_m(T)}}=\frac{\mathrm{V_c(z)}}{\left[1+(1-\mathrm{V_c(z)})3\frac{(\mathrm{K_c(T)-K_m(T)})}{3\mathrm{K_m(T)+4G_m(T)}}\right]} \tag{3}$$

$$\frac{\mathrm{G(z,T)-G_m(T)}}{\mathrm{G_c(T)-G_m(T)}}=\frac{\mathrm{V_c(z)}}{\left[1+(1-\mathrm{V_c(z)})\frac{(\mathrm{G_c(T)-G_m(T)})}{\mathrm{G_m(T)+f(T)}}\right]} \tag{4}$$

$$\frac{\mathrm{\alpha(z,T)-\alpha_m(T)}}{\mathrm{\alpha_c(T)-\alpha_m(T)}}=\frac{(1/\mathrm{K(z,T)})-(1/\mathrm{K_m(T)})}{(1/\mathrm{K_c\,(T)})-(1/\mathrm{K_m(T)})} \tag{5}$$

where

$$\mathrm{f(T)}=\frac{\mathrm{G_m(T)(9K_m(T)+8G_m(T))}}{6(\mathrm{K_m(T)+2G_m(T)})} \tag{6}$$

$\mathrm{K(T)}=\frac{\mathrm{E}}{3(1-\nu)}$ (for both ceramic and metal constituents)

$\mathrm{G(T)}=\frac{\mathrm{E}}{2(1+\nu)}$ (for both ceramic and metal constituents).

Thereafter, over the thickness of FGM plate the effective values of Young's modulus *E(z)* and Poisson's ratio $\nu(z)$ of FGM plate can be calculated using following expressions:

$$\mathrm{E(z,T)}=\frac{9\mathrm{K(z,T)G(z,T)}}{(3\mathrm{K(z,T)+G(z,T)})} \tag{7}$$

$$\nu(\mathrm{z,T})=\frac{(3\mathrm{K(z,T)}-2\mathrm{G(z,T)})}{2(3\mathrm{K(z,T)+G(z,T)})} \tag{8}$$

3 PLASTIC BEHAVIOR OF FGM PLATE

The plastic behavior of FGM plate (i.e., yield strength and plastic tangent modulus of FGM) can be depicted by a homogenized mixture rule, so called TTO model (also called the modified rule of mixtures).

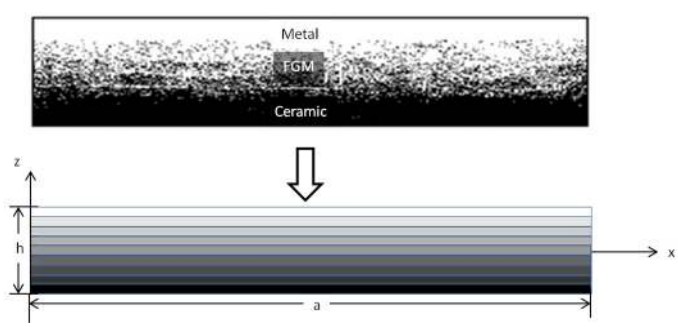

Figure 1: Modeling of actual non-homogeneous FGM plate into a laminate composed of multiple perfectly-bonded homogeneous layers.

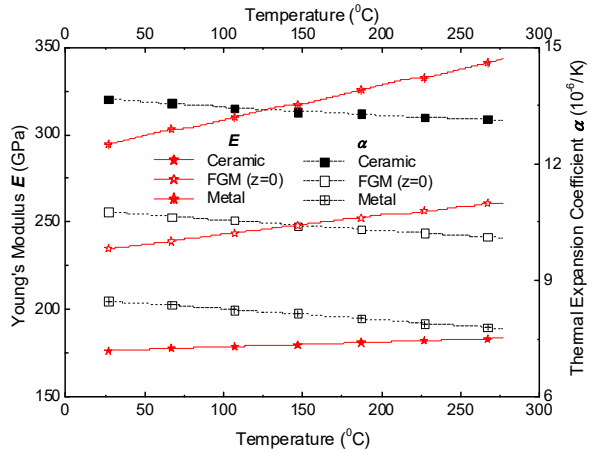

Figure 2: Temperature dependent Young's modulus (E) and thermal expansion coefficient (α).

	Materials	P_0	P_{-1}	P_1	P_2	P_3
E(Pa)	Al_2O_3	349.55e9	0.0	-3.853e-4	4.027e-7	-1.673e-10
	Ni	223.95e9	0.0	-2.794e-4	-3.998e-9	0.0
α(1/K)	Al_2O_3	6.8260e-6	0.0	1.838e-4	0.0	0.0
	Ni	9.9209e-6	0.0	8.705e-4	0.0	0.0

Table 1: Temperature-dependent thermoelastic coefficients for Al_2O_3 and Ni, from (Reddy and Chin, 1998).

	P_0	P_{-1}	P_1	P_2	P_3
σ_y(Pa)	62.81e6	0.0	516.68e3	-8.794e2	-3.565e-1
H(Pa)	-91.75e7	0.0	930.64e4	-15.88e3	75.72e-1

Table 2: Temperature-dependent strength coefficients for Ni, from (Williamson et al., 1995).

The TTO model, initially proposed and used for metal alloys (i.e., Fe-Ni-C) by Tamura et al. (Tamura et al., 1973), has been modified for FGMs by introducing a proper stress transfer parameter (Bocciarelli et al., 2008; Tohgo et al., 2006) and applied by many researchers in the study of FGM. For instance, Jin et al (Jin et al., 2003) investigated the nucleation of plastic crack growth near the interface of metal/ceramic FGM using TTO model. Williamson et al. (Williamson et al., 1995) adopted TTO model to investigate residual stresses developed at the interfaces of bonded Al_2O_3-Ni. Giannakopoulos et al. (Giannakopoulos et al., 1995) investigated the elastoplastic response of Al_2O_3-Ni FGM layer using the incremental theory of plasticity and the stress-strain curves for FGM were drawn by using TTO model. It is to be noticed that the TTO model assumes that the overall failure behavior of two-phase composite containing both brittle and ductile phases is governed by the ductile constituent (Jin et al., 2003). This assumption is also considered to be reasonable in the case of FGMs (containing ceramic: a brittle phase, and metal: a ductile phase) because the ductility and good shear strength induced in the FGM by the metal phase relax the stress concentration induced around the inherited cracks and flaws of ceramics through the plastic defor-

mation and hence, eliminate the possibility of brittle failure of FGM (Bandyopadhyay et al.; Soh et al., 2000).

Based on the assumption that the FGM yields once the metal constituent yields, the TTO model uses q (stress transfer parameter), σ_{ym}(yield strength of metal) and H_m(tangent modulus of metal) to give the overall yield strength and tangent modulus of FGM for predicting the elasti-oplastic response as

$$\sigma_y(z,T) = \sigma_{ym}(T)\left[V_m(z) + \left(\frac{q + E_m(T)}{q + E_c(T)}\right)\frac{E_c(T)}{E_m(T)}(1 - V_m(z))\right] \tag{9}$$

$$H(z,T) = \left\{V_m(z)H_m(T)\frac{q + E_c(T)}{q + H_m(T)} + (1 - V_m(z))E_c(T)\right\} \times \left\{V_m(z)\frac{q + E_c(T)}{q + H_m(T)} + (1 - V_m(z))\right\}^{-1} \tag{10}$$

where the subscripts c and m correspond to the material phases ceramic and metal, respectively; and, q represents the stress transfer parameter, also called stress-to-strain transfer ratio. The value of q, determined numerically or/and experimentally, depends upon the properties of constituent materials as well as on the microstructure interaction in FGM material. For Ni-Al_2O_3 (Giannakopoulos et al., 1995) and TiB/Ti (Jin et al., 2003) FGMs, the value for q is found to be 4.5 GPa, and for FGM containing Al and SiC (Bhattacharyya et al., 2007; Gunes et al., 2011) phases it is determined to be 91.6 GPa. Using the volume fraction of the constituents at a particular thickness coordinate [calculated from Eq. (1)], the temperature dependent yield strength and the temperature dependent tangent modulus of FGM plate at that thickness coordinate are calculated using Eqs. (9)-(10). It is assumed that under the assumption of idealized bilinear hardening behavior of metal, the FGM also follows bilinear plastic response (Giannakopoulos et al., 1995; Williamson et al., 1995) and the values of temperature dependent yield strength σ_{ym} and tangent modulus H_m of Ni are taken from the reference (Williamson et al., 1995).

4 DEFINITION OF ULTIMATE FAILURE OF FGM

The strategy followed to predict the ultimate strength of FGM plate is adopted from the literature wherein the researchers have utilized nonlinear FEM to determine the ultimate strength of elastic-perfectly plastic and bilinear elastic-plastic isotropic homogeneous plates (El-Sawy et al., 2004; Estefen et al., 2016; Ghavami and Khedmati, 2006; Narayanan and Chow, 1984; Paik, 2005; Shanmugam et al., 1999a).

In the present study, FGM plate is subjected to axial compressive load in an incremental manner which causes recoverable elastic stresses and strains within elastic range; however, at relatively large value of load (i.e., beyond yield load) the yielding in FGM plate is followed by recoverable elastic strains as well as irrecoverable plastic strains in the plate. As the load further increases, the proportion of plastic strain reaches to an extent where the plate becomes unstable, because of complete loss in stiffness of plate, to result in ultimate failure of FGM plate; the corresponding load is termed as ultimate failure load. It is to be noted that in the present elastic-plastic analysis the load is applied in small incremental load steps to ensure that the analysis closely follow the actual load-response curve of FGM plate.

5 THERMO-ELASTO-PLASTIC CONSTITUTIVE RELATION

To carry out elastoplastic analysis, the material is assumed to obey the von-Mises yielding criterion, and the corresponding yield surface is assumed to undergo uniform expansion in the stress space with increasing plastic deformations. The yield function can be expressed as:

$$f = \sqrt{3J_2} - \sigma_{Yield} \tag{11}$$

$$J_2 = \frac{1}{6}\left[\left(\sigma_x - \sigma_y\right)^2 + \left(\sigma_y - \sigma_z\right)^2 + (\sigma_x - \sigma_z)^2 + 6\left(\tau_{xy}^2 + \tau_{yz}^2 + \tau_{xz}^2\right)\right] \tag{12}$$

Due to the effect of strain hardening the initial yield surface varies at each stage of plastic deformation and hence the equation of yield surface for a solid undergoing thermo-elasto-plastic deformation can be written as

$$f = f(\sigma, \kappa, T) \tag{13}$$

where κ and T denotes the strain hardening parameter and temperature. After differentiating the f using chain rule of partial differentiation

$$df = \left(\frac{\partial f}{\partial \sigma}\right)^T d\sigma + \frac{\partial f}{\partial \kappa} d\kappa + \frac{\partial f}{\partial T} dT \tag{14}$$

It is known that the hardening parameter (κ) is function of plastic strain (ε_p) and loading history (k), hence the equation of yield surface can be rewritten as

$$df = \left(\frac{\partial f}{\partial \sigma}\right)^T d\sigma + \frac{\partial f}{\partial k}\left(\frac{\partial k}{\partial \varepsilon_p}\right) d\varepsilon_p + \frac{\partial f}{\partial T} dT \tag{15}$$

The variation in plastic strain energy should be zero, to satisfy the equilibrium of solid under small incremental plastic deformation, hence

$$df = \left(\frac{\partial f}{\partial \sigma}\right)^T d\sigma + \frac{\partial f}{\partial k}\left(\frac{\partial k}{\partial \varepsilon_p}\right) d\varepsilon_p + \frac{\partial f}{\partial T} dT = 0 \tag{16}$$

Now the total incremental strain combines the incremental parts of elastic strain ($d\varepsilon_e$), thermal strain ($d\varepsilon_T$), strain due to temperature dependent material properties ($d\varepsilon_{TD}$), and plastic strain ($d\varepsilon_p$)

$$d\varepsilon = d\varepsilon_e + d\varepsilon_T + d\varepsilon_{TD} + d\varepsilon_p \tag{17}$$

By the virtue of Hook's law, the total incremental stress ($d\sigma$), may be written as

$$d\sigma = [D]\left\{d\varepsilon - (d\varepsilon_T + d\varepsilon_{TD} + d\varepsilon_p)\right\} \tag{18}$$

Putting the value of total incremental stress ($d\sigma$) into Eq. (16)

$$df = \left(\frac{\partial f}{\partial \sigma}\right)^T [D]\left\{d\varepsilon - (d\varepsilon_T + d\varepsilon_{TD} + d\varepsilon_p)\right\} + \frac{\partial f}{\partial k}\left(\frac{\partial k}{\partial \varepsilon_p}\right) d\varepsilon_p + \frac{\partial f}{\partial T} dT = 0 \tag{19}$$

The plastic potential function is assumed to be identical to the yield function in the so called associative flow rule given by

$$d\varepsilon_p = d\lambda \frac{\partial f}{\partial \sigma} \tag{20}$$

The components of thermal strain ($d\varepsilon_T$) and strain due to temperature dependent material properties ($d\varepsilon_{TD}$) are given as

$$\begin{aligned} d\varepsilon_T &= \alpha\, dT, \\ d\varepsilon_{TD} &= \frac{\partial [D]^{-1}}{\partial T} \sigma\, dT \end{aligned} \tag{21}$$

$$\left(\frac{\partial f}{\partial \sigma}\right)^T [D] \left(\frac{\partial f}{\partial \sigma}\right) - \frac{\partial f}{\partial k} \left(\frac{\partial k}{\partial \varepsilon_p}\right)^T \left(\frac{\partial f}{\partial \sigma}\right) = \eta^i \tag{22}$$

The substituting Eqs. (20-22) into the Eq. (19) and rearranging the equation to obtain the value of flow variable $d\lambda$.

$$d\lambda = \frac{\left(\frac{\partial f}{\partial \sigma}\right)^T [D] \left\{ d\varepsilon - (\alpha\, dT + \frac{\partial [D]^{-1}}{\partial T} \sigma\, dT) \right\} + \frac{\partial f}{\partial T} dT}{\eta^i} \tag{23}$$

The expression for $d\sigma$ is obtained using Eqs. (20-23) into Eq. (18)

$$\begin{aligned} d\sigma = [D] \left\{ (d\varepsilon) - (\alpha\, T + \frac{\partial [D]^{-1}}{\partial T} \sigma\, T) \right\} \\ - [D] \frac{\partial f}{\partial \sigma} \left\{ \frac{\left(\frac{\partial f}{\partial \sigma}\right)^T [D] \left\{ d\varepsilon - (\alpha\, dT + \frac{\partial [D]^{-1}}{\partial T} \sigma\, dT) \right\} + \frac{\partial f}{\partial T} dT}{\eta^i} \right\} \end{aligned} \tag{24}$$

Rearranging the Eq. (24)

$$d\sigma = \left([D] - \frac{1}{\eta^i} [D] \frac{\partial f}{\partial \sigma} \left(\frac{\partial f}{\partial \sigma}\right)^T [D]\right) \left\{ (d\varepsilon) - \left(\alpha\, T + \frac{\partial [D]^{-1}}{\partial T} \sigma\, T \right) \right\} + \frac{1}{\eta^i} [D] \frac{\partial f}{\partial \sigma} \frac{\partial f}{\partial T} dT \tag{25}$$

The term $\left([D] - \frac{1}{\eta^i} [D] \frac{\partial f}{\partial \sigma} \left(\frac{\partial f}{\partial \sigma}\right)^T [D]\right)$ in Eq. (25) represents the elasto-plastic constitutive matrix $\left[D_{ep}\right]^i$, which finally gives the thermo-elasto-plastic constitutive relationship

$$\left[D_{ep}\right]^i = \left([D] - \frac{1}{\eta^i} [D] \frac{\partial f}{\partial \sigma} \left(\frac{\partial f}{\partial \sigma}\right)^T [D]\right) \tag{26}$$

$$d\sigma = \left[D_{ep}\right]^i \left\{ (d\varepsilon) - \left(\alpha\, T + \frac{\partial [D]^{-1}}{\partial T} \sigma\, T \right) \right\} + \frac{1}{\eta^i} [D] \frac{\partial f}{\partial \sigma} \frac{\partial f}{\partial T} dT \tag{27}$$

6 FEM FORMULATION

The displacement within an element is interpolated by an expression of the form

$$\{a\}^e = [u, \quad v, \quad w, \quad \theta_x \quad \theta_y]^T = \sum_{i=1}^{N} [N_i I_5]\{a_i\} \tag{28}$$

where $\{a\}$ is the value of displacement components at a point within an element; n the number of nodes in an element; N_i the interpolation functions of a Lagrangian element. The variation in Green's strain vector $\Delta\epsilon$ is given in the form of variation in nodal displacements Δa and strain-displacement matrix B

$$\Delta\epsilon = B\Delta a \tag{29}$$

Considering the aforementioned case of thermo-elasto-plastic isotropic hardening case the total incremental strain energy in the element may be written as

$$\Delta U = \frac{1}{2}\int_V \Delta\epsilon'^T \Delta\sigma \, \Delta\epsilon' dV \tag{30}$$

where

$$\Delta\epsilon' = \Delta\epsilon - \Delta\epsilon^T \tag{31}$$

$$\Delta\epsilon^T = \alpha \, \Delta T + \frac{\partial[D]^{-1}}{\partial T}\sigma \, \Delta T + \frac{1}{\eta^i}[D]\left[D_{ep}\right]^{-1}\frac{\partial f}{\partial \sigma}\frac{\partial f}{\partial T}\Delta T$$

Using the values of $\Delta\sigma$ and $\Delta\epsilon'$ from aforementioned Eqs. (37, 39 and 31), we get expression of ΔU in terms of nodal displacement vector

$$\Delta U = \frac{1}{2}\Delta a^T\left(\int_V B^T\left[D_{ep}\right]^i B \, dV\right)\Delta a - \Delta a^T \int_V B^T\left[D_{ep}\right]^i \Delta\epsilon^T \, dV + \frac{1}{2}\int_V \Delta\epsilon^T\left[D_{ep}\right]^i \Delta\epsilon^T \, dV \tag{32}$$

In absence of body forces the external virtual work can be split into two terms related to work done due to tractions at plate surface and at plate edges.

$$\Delta W_{ex}^t = \Delta a^T \int_A N^T \hat{\bar{P}} \, dA + \Delta a^T \int_s N^T \hat{\bar{P}}_e \, ds \tag{33}$$

$$\text{Where} \qquad \hat{\bar{P}} = \left[P_x \quad P_y \quad P_z \quad \bar{M}_x \quad \bar{M}_y\right]^T \tag{34}$$

and the generalized edge forces are given as

$$\hat{\bar{P}}_e = \left[\bar{P}_x^e \quad \bar{P}_y^e \quad \bar{P}_z^e \quad \bar{M}_x^e \quad \bar{M}_y^e\right]^T = \int_{h/2}^{h/2}\left[\left(P_x^e \quad P_y^e \quad P_z^e \quad M_x^e \quad M_y^e\right)dz\right]^T \tag{35}$$

Applying the variational principle for functional $\Delta\Gamma(\Delta a) = \Delta U - \Delta W_{ex}^t$ with respect to Δa we get

$$\left(\int_V B^T\left[D_{ep}\right]^i B \, dV\right)\Delta a - \int_V B^T\left[D_{ep}\right]^i \Delta\epsilon^T \, dV - \int_A N^T \hat{\bar{P}} \, dA - \int_s N^T \hat{\bar{P}}_e \, ds = 0 \tag{36}$$

Finally the following matrix equations are obtained

$$[K]\Delta a = \Delta R \tag{37}$$

where $[K^T]$ is tangent stiffness matrix given by

$$[K] = \int_V B^T [D_{ep}]^i B \, dV \tag{38}$$

ΔR in Eq. (37) is incremental external load vector due to combined mechanical loading(ΔR_M) and thermal loading(ΔR_T) hence given by

$$\begin{aligned} \Delta R &= \Delta R_M + \Delta R_T \\ \Delta R_M &= \int_A N^T \tilde{P} \, dA + \int_s N^T \tilde{P_e} \, ds \end{aligned} \tag{39}$$

7 SOLUTION PROCEDURE

In the present study, the nonlinear finite element method is used to investigate the nonlinear thermomechanical stability and failure behavior of FGM plate with temperature dependent material properties. Eight-noded shell element (SHELL281), possessing six degrees of freedom (three translations and three rotations in x, y and z directions) per node and especially designed for modeling the large deformation plastic behavior of layered structures, is used to mesh the FGM plate.

Using APDL (i.e., ANSYS Parametric Design Language) a macro is written for conducting the thermomechanical elastoplastic postbuckling analysis of FGM plate, in the following two stages:
In the first stage, the linear buckling analysis is performed to find the critical buckling load and corresponding mode shape by following the below procedure.

Initially, the undeformed geometry of structure is loaded with the nominal arbitrary level of the load F_0 (also called reference load) and the linear analysis is performed to find out the initial stress stiffness matrix $K_\sigma[F_0]$. Thereafter, the total stiffness of plate at some applied load F_0 is written as:

$$K_{total}(T, F_0) = [K(T)] + K_\sigma[F_0] \tag{40}$$

where,
$[K(T)]$ = Conventional small deformation and temperature dependent stiffness matrix.
$K_\sigma[F_0]$ = Initial stress stiffness matrix that accounts for the effect of existing state of stress σ due to applied load F_0 in the plate and it is independent of material properties.

Thereafter, the total stiffness matrix of plate corresponding to some other level of load ΛF_0 is determined as:

$$K_{total}(T, \Lambda F_0) = [K(T)] + K_\sigma[\Lambda F_0] = [K(T)] + \Lambda K_\sigma[F_0] \tag{41}$$

where Λ corresponds to buckling load multiplier. The equilibrium equation just before the bifurcation buckling point of the plate corresponding to applied load level ΛF_0 and displacement vector $\{u_0\}$ may be written as

$$([K(T)] + \Lambda K_\sigma[F_0])\{u_0\} = \Lambda F_0 \tag{42}$$

As it is evident that at buckling point, the plate exhibits increase in its displacements (say, δu) without any increase in the applied load. Hence at the point of bifurcation, the corresponding equilibrium equation can be written by

$$([K(T)] + \Lambda K_\sigma[F_0])\{u_0 + \delta u\} = \Lambda F_0 \tag{43}$$

The required eigenvalue equation to determine the buckling load and the corresponding mode shape for the plate can be obtained by subtracting Eq.(42) from Eq.(43) as:

$$([K(T)] + \Lambda K_\sigma[F_0])\{\delta u\} = 0 \tag{44}$$

Hence, to solve Eq. (44) we take

$$|[K(T)] + \Lambda K_\sigma[F_0]| = 0 \tag{45}$$

to obtain the critical buckling load as the lowest eigenvalue (i.e., the first value of Λ) and the corresponding mode shape as the eigenvector $\{\delta u\}$ (El-sawy and Nazmy, 2001).

In the second stage, a nonlinear large displacement elastioplastic static analysis is performed to investigate the postbuckling and failure characteristics of the FGM plate.

The nonlinear finite element analysis is performed using an incremental procedure in which the load is applied gradually in stepwise manner and the corresponding deformation is obtained by updating the temperature dependent material properties at each load step. It is well known that finding postbuckling path using incremental analysis requires some type of imperfection in the structure, lacking which incremental analysis would trace the linear solution only without showing any bifurcation buckling point (Barbero, 2013). As the critical buckling load corresponding to the first mode shape is the lowest; therefore, to initiate bifurcation buckling and to obtain postbuckling path, the mesh is modified by superimposing imperfection equal to b/1000 (where, b represents width of the plate) in the shape of the first mode, obtained by eigen buckling analysis carried out in the first stage.

While solving nonlinear algebraic equations obtained in finite element analysis, the Newton-Raphson (N-R) method is used. While using Newton-Raphson method, the tangent stiffness matrix K_T (the relationship between the incremental load and the associated displacement) comprises of three matrices: conventional small deformation linear stiffness matrix, initial stress stiffness matrix and non-linear stiffness matrix (due to involved geometry and material nonlinearity). In the Newton-Raphson method, for ith iteration we have:

$$[K_i^T]\{\Delta a_i\} = \{F^a\} - \{F_i^{nr}\} \tag{46}$$

where
$[K_i^T]$ = tangent stiffness matrix at ith iteration,
$\Delta a_i = a_{i+1} - a_i$, incremental displacement vector
$\{F^a\}$ = external applied load vector
$\{F_i^{nr}\}$ = restoring internal force vector

Incremental Elastic-plastic solution of FGM plate

1. The material properties E and a, and the yield strength $\sigma_{Yield}(z,T)$ and tangent modulus H at each layer of FGM plate are evaluated for current temperature T_i at ith time step and utilized to compute the temperature dependent constitutive matrix $[D(T)]_i$ at present time step.

2. Initially the displacements (a_0), strains (ϵ_0) and stresses (σ_0) are known from previous load step or are zero.

3. Determine the elasto-plastic constitutive matrix from previously known variables utilizing the Eq. (26).

4. Apply the boundary conditions and obtain the incremental displacements (Δa) by solving the Eq. (42).

5. The Eq. (32) can be utilized to obtain the incremental strains $(\Delta\epsilon)$ with the aid of calculated incremental displacements (Δa). The incremental stresses $(\Delta\sigma)$ are calculated by Eq. (32).

6. Total stresses and strains are updated as

$$\sigma_n = \sigma_0 + \Delta\sigma$$
$$\epsilon_n = \epsilon_0 + \Delta\epsilon$$

7. The updated stresses and strains are substituted in Eq. (16) to perform plasticity check

a. If $f(\sigma_n) < 0$ there is elastic deformation and go-to step 8

b. If $f(\sigma_n) > \sigma_{Yield}$ and $f(\sigma_0) \geq \sigma_{Yield}$ there is plastic deformation and stress correction procedure is applied to define the corrected stress σ_{cn}

Stress Correction Procedure

Let $\sigma_m = \sigma_0 + \frac{\Delta\sigma}{2}$ *and* $\epsilon_m = \epsilon_0 + \frac{\Delta\epsilon}{2}$

$$\Delta\sigma = \left[D_{ep}(\sigma_m, \epsilon_m)\right]\Delta\epsilon^*$$

where $\Delta\epsilon^* = \Delta\epsilon - \Delta\epsilon_{tn}$

$$\Delta\epsilon_{tn} = \alpha\,\Delta T + \frac{\partial[D]^{-1}}{\partial T}\sigma\,\Delta T + \frac{1}{\eta^i}[D]\left[D_{ep}\right]^{-1}\frac{\partial f}{\partial\sigma}\frac{\partial f}{\partial T}\Delta T$$

then the corrected stress value is given by $\sigma_{cn} = \sigma_0 + \Delta\sigma$

c. If $f(\sigma_n) > \sigma_{Yield}$ and $f(\sigma_0) < \sigma_{Yield}$ this is critical case in which the plasticity is occurred within current load increment, the stresses and strains are updated as $\sigma_n = \sigma_0 + (1-\varphi)\Delta\sigma$

$$\epsilon_n = \epsilon_0 + (1-\varphi)\Delta\epsilon$$

here $\varphi = \frac{f(\sigma_0)}{f(\sigma_0) - f(\sigma_n)}$

8. The nodal coordinates are updated by adding corresponding values of nodal displacements.

9. Go-to step 1 for next load increment.

Table 3: Solution procedure for elastioplastic analysis of FGM plate.

The right-hand side of Eq. (45), called residual or out-of-balance load vector [say $\{\aleph\}$], is to be minimized by iterative procedure, till the following convergence criterion is satisfied.

$$\|\{\aleph\}\| < \varepsilon\aleph_{\mathrm{ref}}$$

where the value of tolerance (i.e., ε) is taken as 0.001, and $\mathrm{R_{ref}}$ is considered to be equal of $\|\{\mathrm{R^a}\}\|$. $\|.\|$ represents a vector norm that define the square root of the sum of the squares of value of the enclosed terms. Since the elastoplastic constitutive equations depend upon the present level of stresses and the deformation history, hence for predicting the elastoplastic buckling and postbuckling behavior of FGM plate, incremental iterative procedure as given in Table 3 is followed.

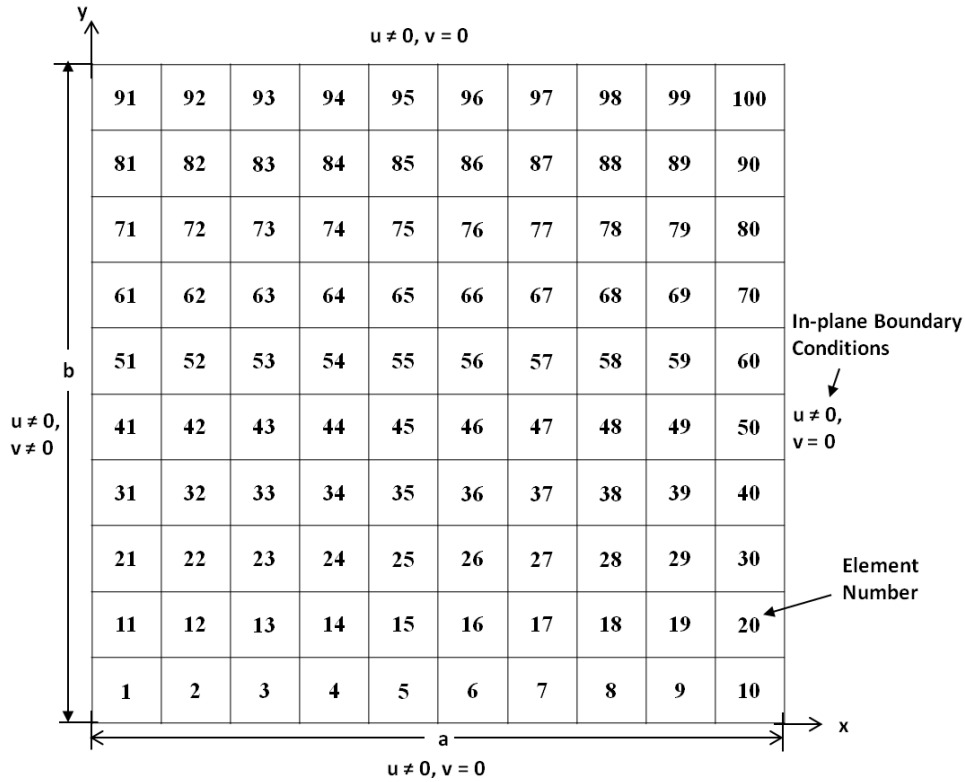

Figure 3: Meshing of a typical FGM plate along with in-plane boundary conditions.

8 PROBLEM DEFINITION

In the present study, a rectangular FGM plate of dimension ($a \times b \times h$), is studied to investigate the thermomechanical buckling, postbuckling and failure characteristics of the elastoplastic FGM plate. The FGM plate is assumed to be made of two constituents: Al_2O_3 (i.e., ceramic phase) and Ni (i.e., metallic phase). The temperature-dependent material properties of FGM are evaluated by Eq. (2) using temperature-dependent thermoelastic coefficients for the Al_2O_3 and Ni phases of FGM given in Table 1. Similarly, the temperature-dependent strength coefficients for Ni (i.e., metallic phase) are provided in Table 2 to determine temperature-dependent yield strength σ_{ym} and tangent modulus H_m of Ni using Eq. (2).

8.1 Boundary and Loading Conditions

The current study is carried out for a simply-supported FGM plate with the following flexural boundary conditions:

$$w = 0, \theta_x \neq 0, \theta_y = 0 \text{ at } x = 0 \,\&\, a$$
$$w = 0, \theta_x = 0, \theta_y \neq 0 \text{ at } y = 0 \,\&\, b$$

The prescribed in-plane displacements (i.e., u and v) at various plate edges for uniaxial and bi-axial load conditions are as follows:

For uniaxial loading:

$$\mathrm{u} \neq 0, \mathrm{v} \neq 0 \text{ at } \mathrm{x} = 0 \,\&\, a \,;\; u \neq 0, v = 0 \; at \; y = 0 \,\&\, b$$

For biaxial loading:

$$\mathrm{u} \neq 0, \mathrm{v} \neq 0 \text{ at } \mathrm{x} = 0 \,\&\, a \,;\; u \neq 0, v \neq 0 \text{ at } \mathrm{y} = 0 \,\&\, b$$

Where u, v and w are the displacement components in x, y and z directions, respectively; θ_x and θ_y represent the mid-plane rotation of the normal about the y and x axes, respectively.

At a particular temperature, the in-plane uniformly distributed compressive load is applied on edges $x = 0 \,\&\, a$ for uni-axial compression, and on edges $x = 0 \,\&\, a$, $y = 0 \,\&\, b$ for bi-axial compression.

Results for buckling and failure loads, and the transverse deflection are presented in the following non-dimensionalized forms:

In-plane buckling and failure load: $\frac{N_{x\,(or\,y)}\, b^2}{E_c h^3}$ (represented as λ);

Maximum transverse deflection: $\frac{\mathrm{w_{max}}}{\mathrm{h}}$;

Magnitude of maximum plastic strain: $\left(\frac{2}{3}\varepsilon_p : \varepsilon_p\right)^{1/2}$

where $\mathrm{E_c}$ is the Young's modulus of ceramic; h represents the thickness of FGM plate; b is the width of plate; $N_{x\,(or\,y)}$ is the in-plane compressive load in x- direction (or y-direction) per unit edge length, applied at $x = a$ (or $y = b$), w_{max} is the maximum transverse deflection, and $\varepsilon_p : \varepsilon_p$ is the scalar product of the plastic strain tensor corresponding to failure point.

9 CONVERGENCE STUDY

To fix the number of elements in the finite element mesh of FGM plate and the number of layers [to model the actual non-homogeneous FGM with continuously varying properties (only in thickness direction) plate into a laminated plate with multiple perfectly-bonded layers of isotropic material having layer-wise constant composition, but varying along thickness], a convergence study was conducted for a simply-supported FGM plate using meshes of 81, 100, and 121 elements having 10, 20 and 30 layers. The convergence of buckling and failure loads was checked for FGM ($n = 1$) square plate with $b/h = 100$ under uni-axial compression and constant temperature rise of 100°C. Results of convergence study are shown in Table 4.

No. of elements	**No. of layers**					
(along x ×	10		20		30	
along y)	λ	λ^*	λ	λ^*	λ	λ^*
9×9	0.60305	3.98510	0.56602	3.740401	0.55280	3.42578
10×10	0.60741	3.90539	0.55280	3.460745	0.54174	3.39153
11×11	0.59247	3.91518	0.54721	3.425788	0.53741	3.364398

Table 4: Convergence study for critical buckling load $\left(\boldsymbol{\lambda = \frac{N_x b^2}{E_c h^3}}\right)$ and failure load $\left(\boldsymbol{\lambda^* = \frac{N_{fail} b^2}{E_c h^3}}\right)$ for simply supported FGM plate under uni-axial compression and constant temperature rise of $\Delta T = 100$, for $b/h = 100$ and $n = 1$.

b/t	Normalized Ultimate Strength $\left(\frac{\sigma_u}{\sigma_y}\right)$	
	Shanmugam et al. (1999)	**Present Study**
60	0.72	0.68
50	0.81	0.84
40	0.90	0.94
30	0.95	0.99
20	1.01	1.01

Table 5: Comparison between the ultimate strength ratio, computed in present study and the results of Shanmugam et al.(1999).

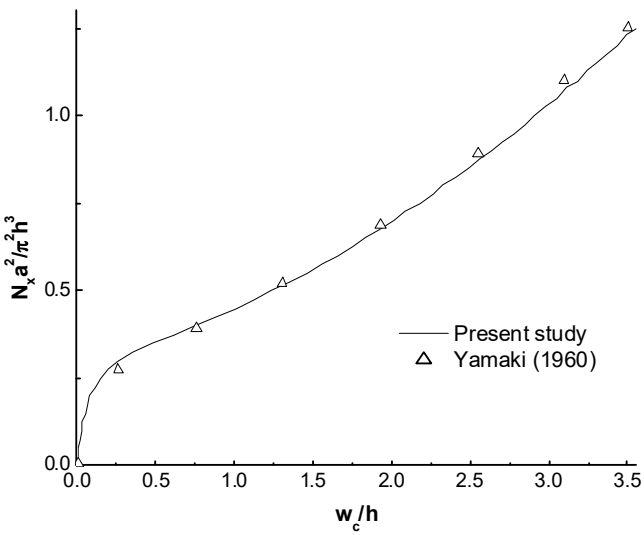

Figure 4: Comparison of postbuckling load-deflection curves for an isotropic simply supported square plate under uniaxial compression obtained in the present study with Yamaki (Yamaki, 1960).

It can be seen from Table 4 that results for buckling and failure loads for FGM plate are converged reasonably for the mesh of 100 elements (i.e., 10 × 10) when modeled with 20 layers. Schematic of finite element meshes along with element and node-numbering schemes for a typical FGM plate is shown in Figure 3.

10 VERIFICATION OF RESULTS

The accuracy and effectiveness of the present method is checked by comparing the results obtained following the present procedure with those available in the literatures (Shanmugam et al., 1999b; Shen, 2007; Yamaki, 1960). Elastic buckling load and postbuckling response of a thin simply-supported square plate (with b/h = 120) made of homogeneous and isotropic material (E = 68.189 GPa and ν = 1/3) under uni-axial compression are compared with that reported by Yamaki (Yamaki, 1960). It can be seen in Figure 4 that results agree well with that of Yamaki (Yamaki, 1960). In addition, the results for thermal buckling load and postbuckling equilibrium path are also

validated with that reported by Shen (Shen, 2007) for a thick simply-supported square plate (with b/h =10) made of homogeneous and isotropic elastic-material. A good agreement is achieved between the results of current study and that of Shen (Shen, 2007), as depicted in Figure 5. Furthermore, the validity of present procedure for elastoplastic analysis is verified by comparing the ultimate strength ratio (defined as the ratio of ultimate strength to yield strength of the material, i.e., σ_u/σ_y) of a simply-supported plate obtained in the present study with that reported by Shanmugam et al. (Shanmugam et al., 1999b).

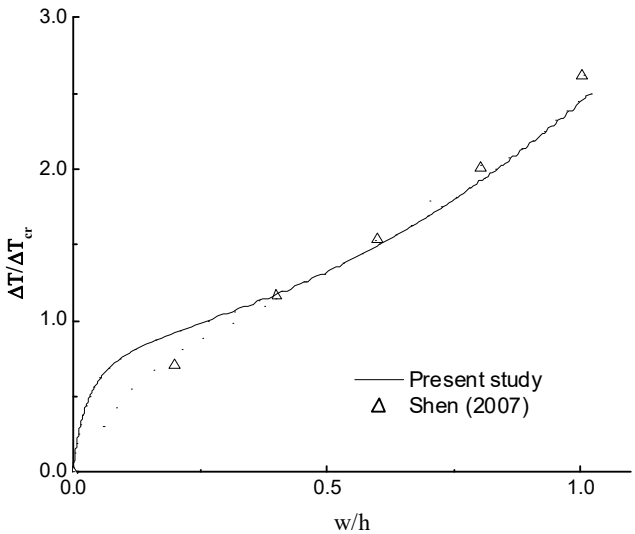

Figure 5: Comparison of postbuckling load-deflection curves for an isotropic simply supported moderately thick (b/h=10) square isotropic plate under constant temperature rise obtained in the present study with Shen (Shen, 2007).

The material (i.e., A572 Grade 50 steel with Young's modulus, E = 207 GPa, Poisson's ratio, v = 0.3 and Yield strength, σ_y= 343 MPa) of the plate is considered to be isotropic, homogeneous, elastic and perfectly plastic, as assumed in Ref. (Shanmugam et al., 1999b). Table 5 shows a good concurrence between the results of present study with the results reported by Shanmugam et al. (Shanmugam et al., 1999b).

11 NUMERICAL RESULTS AND DISCUSSION

Numerical study is conducted to analyze the elastoplastic buckling, postbuckling path and failure characteristics of simply-supported FGM plate under combined themomechanical loading condition. Effects of material inhomogeneity (i.e., power exponent n), aspect ratio (i.e., a/b), slenderness ratio (i.e., b/h), and loading conditions (i.e., uniaxial and biaxial loading) on the buckling load, postbuckling path, yielding load, maximum plastic strain and failure load of FGM plate is investigated. A Ni/Al_2O_3 FGM plate with temperature dependent material properties is considered and graded as per Mori-Tanaka model as specified in Section 2.2 [i.e., using the volume fraction of the constituents at a particular value of thickness coordinate (calculated using Eq. (1)), the Young's modulus and the coefficient of thermal expansion of FGM plate at that thickness coordinate are calculated using

Eqs. (3)-(8)]. However, the effect of temperature dependence of material properties (i.e., Young's modulus and thermal expansion coefficient) is considered as a nonlinear function of temperature as per Eq. (2).

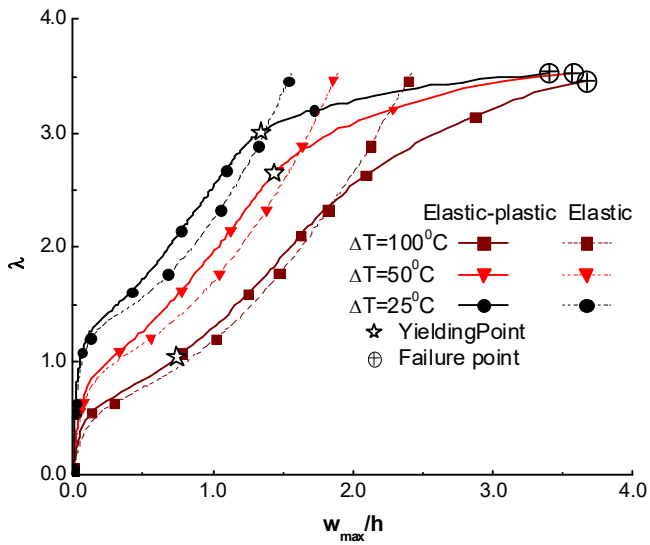

Figure 6: Comparison of elastic and elastic-plastic postbuckling paths for FGM plate under uni-axial compression and constant temperature rise.

It is to mention that unless otherwise stated the FGM plate is graded linearly with power law index unity (i.e., $n = 1$) and the slenderness ratio of FGM plate is kept 100.

The effect of plasticity on nonlinear thermomechanical buckling and postbuckling behavior of FGM square plate (of side 1 m) having temperature dependent (TD) material properties is studied. A simply-supported FGM plate ($n = 1$) under uniaxial mechanical compression loading and uniform temperature rise (i.e., $\Delta T = 25°C, 50°C \text{ and } 100°C$) is considered. The corresponding plots of elastic and elastoplastic buckling and postbuckling paths are shown in Figure 6. The yield and failure points are also marked in the Figure 6 for the cases of elastoplastic studies. It can be seen from Figure 6 that the postbuckling paths for both elastic and elastoplastic FGM plate are strongly dependent on temperature rise (i.e., ΔT) and for a particular value of mechanical load, both elastic and elastoplastic FGM plate exhibit an increase in the value of transverse deflection with the increase in temperature. This response is caused by the high thermal load as well as by the reduced stiffness of FGM plate at high temperature because of the inverse dependence of Young's modulus on temperature (reduction in Young's modulus with increase in temperature) and the direct proportionality of thermal expansion coefficient with temperature, as shown in Figure 2. It can also be observed from Figure 6 that postbuckling paths of FGM plate are greatly affected by the plasticity, as it is evident from the considerable difference in postbuckling paths of elastic and elastoplastic FGM plates. Figure 6 also depicts that irrespective of increase in applied thermal and mechanical loadings, the FGM plate with elastic material properties exhibits only stable equilibrium path, whereas the elastoplastic FGM plate shows destabilizing response after the point of maximum postbuckling strength (also called ultimate failure point) because the behavior of elastoplastic FGM

plate is dominated by plasticity after the point of intersection of postbuckling curves for elastic and elastoplastic FGMs.

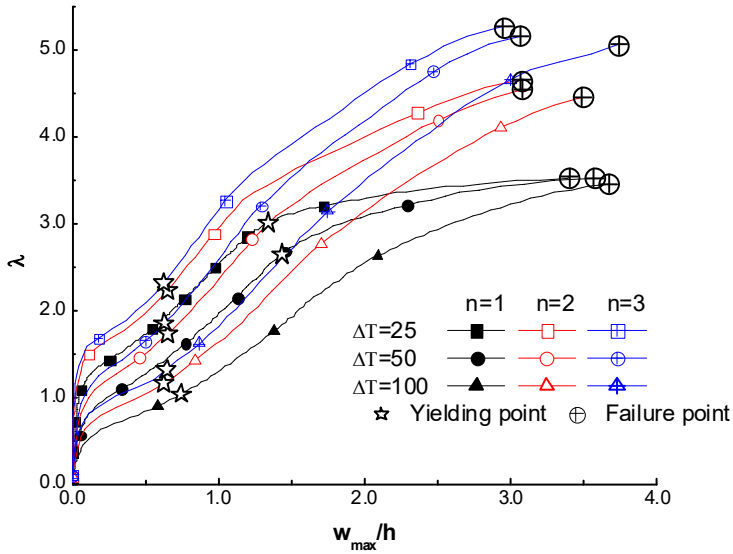

Figure 7: Effect of material gradation on elastic-plastic buckling, postbuckling and failure behavior of Ni/Al_2O_3 FGM plate under uni-axial compression and constant temperature rise.

The effect of material property variation [through the thickness obtained by varying volume fraction using Eq. (1) for different values of exponent n (i.e., 1, 2, and 3)] on elastoplastic buckling and postbuckling responses of simply-supported FGM square plate under uniaxial mechanical compression loading and uniform temperature rise (i.e., $\Delta T = 25℃, 50℃$ and $100℃$) is studied.

The corresponding postbuckling paths are plotted in Figure 7. It is to mention here that the yielding point on a particular load-deflection curve corresponds to the minimum value of the load at which elastic to plastic transition of the metallic phase present anywhere in the FGM takes place, whereas the excessive plasticity preceding the failure load point on a particular load-deflection curve causes the complete loss of load carrying capacity of the FGM plate beyond this point.

It can be observed from Figure 7 that for all values of power law exponent n the FGM plate looses its postbuckling strength (at a particular value of maximum transverse deflection) considerably due to increase in uniform temperature rise (ΔT). Moreover, at large temperature rise the plastic flow in FGM plate spreads more rapidly prompting ultimate failure at a lower value of mechanical load. Figure 7 also show that the ultimate load carrying capacity of FGM plate increases with the increase in value of power law index for all values of uniform temperature rise. This finding is attributed to the fact that at higher value of n, proportion of ceramic (i.e., Al_2O_3), possessing higher thermal resistance, is increased which in turn causes this increase in ultimate failure load of FGM. Further, the effect of plastic flow in FGM plate is more prominent for $n = 1$ that corresponds to a higher metal proportion at a particular thickness coordinate than $n = 2$ & 3, and because of this

effect the FGM plate with $n = 1$ would fail at a lower value of mechanical load for a given uniform temperature rise.

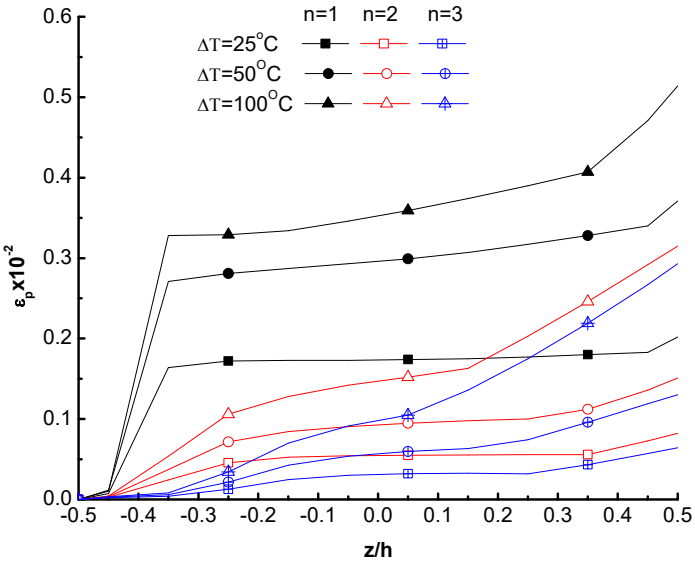

Figure 8: The accumulated plastic strain as a function of thickness for FGM plate with different material gradation profile (i.e., n) under uniaxial compression and constant temperature rise.

Furthermore, the effect of equivalent plastic strain developed across the thickness of FGM plate at a particular value (equal to the failure load for FGM with $n = 1$) of thermomechanical loading is compared for different values of exponent n (i.e., 1, 2, and 3), and the corresponding plots are drawn in Figure 8. It is necessary to mention here that the FGM plate comprises of pure ceramic at bottom (i.e., at z/h = -0.5), whereas top (i.e., at z/h = +0.5) is constituted with pure metallic phase. For a particular value of n, the plastic flow is observed to be more dominating in the upper region of the FGM plate (which corresponds to a high metal proportion) with peak value of equivalent plastic strain noted at the top of the FGM plate, whereas at the lower part of the FGM plate, plasticity is minimum with zero plastic strain at the bottom, and at particular thickness point, the plasticity effect is more pronounced in the case of FGM plate with n = 1. Further, it is also evident from Figure 8 that irrespective of value of n, the effect of higher thermal environment is to provoke more plasticity effects in the FGM plate.

The effects of uni-axial and biaxial loading conditions on elastoplastic buckling and postbuckling behavior and failure of FGM square plate under uniform temperature rise (i.e., ΔT) is examined, and the postbuckling paths for different load ratios (i.e., N_y/N_x) are plotted in Figure 9. The corresponding values of buckling load, yielding stress, failure load and maximum plastic strain are given in Table 6. The results show that for all values of temperature rise, the maximum values of buckling load, postbuckling strength (for a particular value of deflection) and failure load are obtained for plate under uni-axial compression (i.e., for $N_y/N_x = 0$).

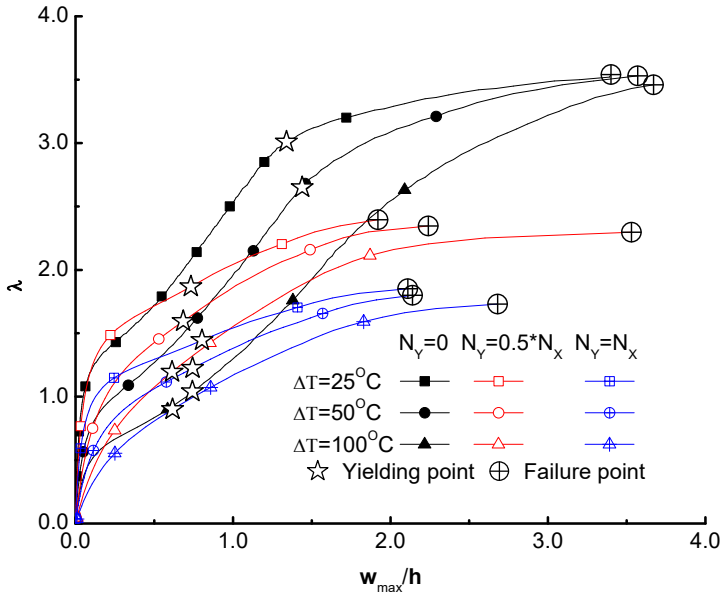

Figure 9: Elastic-plastic buckling and postbuckling behavior of FGM (for n = 1) plate under combined in-plane compressive load and constant temperature rise.

The postbuckling load-deflection curves become significantly lower and the plasticity commences at a lower value of yield load with the increase in N_y/N_x ratio.

To study the effect of aspect ratio, the slenderness ratio is fixed at 100, and for a fixed width (b = 1 m), the different aspect ratios (i.e., 1, 2, and 3) are obtained by varying the length of the plate, and while studying the effect of slenderness ratio, different values of slenderness ratios (i.e., 50,100 and 200) are obtained by varying the thickness of a square (of side 1 m) FGM plate. The corresponding values of buckling load, yielding load, failure load and equivalent plastic strains for different aspect ratios and slenderness ratios are presented in Tables 7 and 8, respectively.

It is necessary to mention here that while carrying out the study on the effects of aspect and slenderness ratios, the number of elements and number of layers in FGM plate were increased proportionately based on the convergence study conducted in Section 3 to get the converged results. It can be seen from Table 7 that for all values of temperature rise (ΔT) buckling and postbuckling strengths are found to be decreased with the increase in aspect ratio, and the highest buckling and postbuckling strengths are obtained for a square FGM plate (i.e., for a/b =1).

A monotonic decrement in the absolute values of buckling load, yielding load and failure load with increase in the slenderness ratio of FGM plate can be noticed from Table 8. Moreover irrespective of value of temperature rise, thick FGM plate exhibits a large value of plastic strain at the time of ultimate failure. It can also be noticed by Table 8 that for all values of slenderness ratios the increase in temperature rise (ΔT) causes reduction in buckling and postbuckling strengths of FGM plate caused by more plastic flow.

N_y/N_x	ΔT	Buckling load (λ_b)	Yielding load (λ_y)	Failure load (λ_f)	Accumulated Max. plastic strain ($\varepsilon_p \times 10^{-2}$)
0	25	1.06	3.01	3.54	0. 20
	50	0.83	2.65	3.53	0. 37
	100	0.55	1.04	3.46	0. 51
0.5	25	1.05	1.87	2.37	0. 11
	50	0.80	1.58	2.33	0. 16
	100	0.49	1.19	2.27	0. 34
1	25	1.00	1.44	1.84	0.14
	50	0.64	1.21	1.78	0.15
	100	0.40	0.89	1.71	0.27

Table 6: Effects of loading (N_y/N_x) on buckling, yielding and failure characteristics of the rectangular simply supported FGM plate under uni-axial compression and constant temperature rise.

a/b	ΔT	Buckling load (λ_b)	Yielding load (λ_y)	Failure load (λ_f)	Max. plastic strain ($\varepsilon_p \times 10^{-2}$)
1	25	1.06	3.01	3.54	0. 20
	50	0.83	2.65	3.53	0. 37
	100	0.55	1.04	3.46	0. 51
2	25	0.86	2.40	3.33	0.11
	50	0.52	1.63	3.26	0.19
	100	0.32	0.96	3.22	0.39
3	25	0.85	2.32	3.32	0.11
	50	0.50	1.64	3.29	0.23
	100	0.32	0.97	3.19	0.39

Table 7: Effects of aspect ratio (a/b) on buckling, yielding and failure characteristics of the rectangular simply supported FGM plate under uni-axial compression and constant temperature rise.

b/h	ΔT	Buckling load (kN)	Yielding load (kN)	Failure load (kN)	Max. plastic strain ($\varepsilon_p \times 10^{-2}$)	$\frac{w_{max}}{h}$
50	25	2401.12	2568.64	5835.28	2.89	3.21
	50	2317.36	2515.64	5830.28	2.94	3.24
	100	2290.36	2291.0	5807.36	2.95	3.35
100	25	369.94	1050.49	1235.46	0. 20	3.54
	50	289.67	924.85	1231.97	0. 37	3.57
	100	191.95	362.96	1207.54	0. 51	3.67
200	25	47.6	171.7	335	0.07	3.71
	50	29.07	117.3	322	0.10	3.92
	100	19.38	71.06	305	0.32	4.21

Table 8: Effects of slenderness ratio (b/h) on absolute values of buckling, yielding and failure loads of simply-supported rectangular FGM plate under uni-axial compression and constant temperature rise.

12 CONCLUSIONS

A study on non-linear finite element analysis of Ni/Al_2O_3 FGM plate under in-plane compression caused by mechanical compression and uniform temperature rise is conducted. The volume fraction of FGM constituents (ceramic and metal) is assumed to follow a simple power law distribution in the thickness direction. The actual non-homogeneous FGM plate with continuously varying properties along thickness is modeled as a laminate composed of multiple perfectly-bonded layers of isotropic material having layer-wise constant (i.e., homogeneous) composition. At the mid of a particular layer, thermoelastic properties (i.e., elastic constants and thermal expansion coefficients) of FGM are calculated using Mori-Tanaka homogenization scheme, whereas the yielding strength is calculated using TTO model. The nonlinear temperature dependent thermoelastic material properties are also incorporated into the model. The finite element formulation is based on the first-order shear deformation theory and the von-Karman's nonlinear kinematics, and the non-linear equations are solved using Newton-Raphson method. After validating the results of present formulation with the available results in literature, the effects of plasticity, material inhomogenity and thermomechanical loading conditions on elastoplastic buckling, postbuckling and collapse behavior of FGM plate is analyzed under the framework of J_2 deformation theory associated with the isotropic hardening flow rule.

Based on the present work, the following important conclusions are drawn.

- Postbuckling response of FGM plate is found to be greatly affected by the plasticity consideration. FGM plate with elastic material properties exhibits only stable equilibrium path, whereas the elastoplastic FGM plate shows destabilizing response after the point of maximum postbuckling strength, also called ultimate failure point.
- Along the thickness of FGM plate, the effect of plastic flow is observed to be more dominating in the metal rich portion of FGM plate (i.e., upper region of the FGM plate) as compared to the ceramic rich lower region.
- The effect of rise in temperature difference (i.e., ΔT) is to develop more plastic strain, irrespective of the value of material gradation index n and the mechanical loading condition.
- The buckling and postbuckling strengths of elastoplastic FGM plate are found to be significantly affected by its material gradation profile; FGM plate with higher ceramic proportion depicted higher buckling and postbuckling strengths.
- The effect of biaxial loading is to reduce the buckling load, postbuckling strength (for a particular value of deflection), and yielding and failure loads, for all values of temperature difference.
- Buckling, yielding and ultimate failure loads of FGM plate are found to decrease with the increase in aspect ratio as well as slenderness ratios of the plate. The failure of thick FGM plate is occurred due to large plastic flow, whereas thin FGM plate shows excessive out of plane deflection at the time of failure.

Acknowledgement

The authors acknowledge the use of ANSYS FE software available with Computer Center, IIT Kanpur through Prof. Shakti S Gupta, Mechanical Engineering Department, IIT Kanpur.

References

Arbocz, J., maggiori, C. italiana dei superiori, 1987. Buckling and post-buckling: four lectures in experimental, numerical, and theoretical solid mechanics based on talks given at the CISM-meeting, held in Udine, Italy, September 29-October 3, 1985. Springer-Verlag.

Bakker, M.C.M.Ã., Rosmanit, M., Hofmeyer, H., 2009. Thin-Walled Structures Prediction of the elasto-plastic post-buckling strength of uniformly compressed plates from the fictitious elastic strain at failure 47, 1–13.

Bandyopadhyay, A., Atisivan, R., Kuhn, G., Yeruva, S., n.d. Mechanical Properties of Interconnected Phase Alumina-Al Composites 24–31.

Barbero, E.J., 2013. Finite element analysis of composite materials using ANSYS®. CRC Press.

Bazant, Z.P., Cedolin, L., Hutchinson, J.W., 1993. Stability of Structures: Elastic, Inelastic, Fracture, and Damage Theories, Journal of Applied Mechanics.

Benveniste, Y., 1987. A new approach to the application of Mori-Tanaka's theory in composite materials. Mech. Mater. 6, 147–157.

Bhattacharyya, M., Kapuria, S., Kumar, a. N., 2007. On the Stress to Strain Transfer Ratio and Elastic Deflection Behavior for Al/SiC Functionally Graded Material. Mech. Adv. Mater. Struct. 14, 295–302.

Bi, R., Fu, Y., Tian, Y., Jiang, C., 2014. Buckling and postbuckling analysis of elasto-plastic fiber metal laminates. Acta Mech. Solida Sin. 27, 73–84.

Birman, V., 1995. Stability of functionally graded hybrid composite plates. Compos. Eng. 5, 913–921.

Birman, V., Byrd, L.W., 2007. Modeling and Analysis of Functionally Graded Materials and Structures. Appl. Mech. Rev. 60, 195.

Bocciarelli, M., Bolzon, G., Maier, G., 2008. A constitutive model of metal-ceramic functionally graded material behavior: Formulation and parameter identification. Comput. Mater. Sci. 43, 16–26.

Cinefra, M., Soave, M., 2011. Accurate Vibration Analysis of Multilayered Plates Made of Functionally Graded Materials. Mech. Adv. Mater. Struct. 18, 3–13.

Duc, N.D., Tung, H. V, 2010. Mechanical and thermal postbuckling of shear-deformable FGM plates with temperature-dependent properties. Mech. Compos. Mater. 46, 461–476.

Durban, D., Zuckerman, Z., 1999. Elastoplastic buckling of rectangular plates in biaxial compression/tension. Int. J. Mech. Sci. 41, 751–765.

El-sawy, K.M., Nazmy, A.S., 2001. Effect of aspect ratio on the elastic buckling of uniaxially loaded plates with eccentric holes 39, 983–998.

El-Sawy, K.M., Nazmy, A.S., Martini, M.I., 2004. Elasto-plastic buckling of perforated plates under uniaxial compression. Thin-Walled Struct. 42, 1083–1101.

Estefen, S.F., Chujutalli, J.H., Soares, C.G., 2016. Influence of geometric imperfections on the ultimate strength of the double bottom of a Suezmax tanker. Eng. Struct. 127, 287–303.

Fu, Y., Shao, X., Chen, Y., 2014. Elasto-plastic buckling and post-buckling analysis of sandwich plates with functionally graded metal-metal face sheets and interfacial damage. Appl. Math. Mech. 35, 325–344.

Ghavami, K., Khedmati, M.R., 2006. Numerical and experimental investigations on the compression behaviour of stiffened plates. J. Constr. STEEL Res.

Giannakopoulos, a. E., Suresh, S., Finot, M., Olsson, M., 1995. Elastoplastic analysis of thermal cycling: layered materials with compositional gradients. Acta Metall. Mater. 43, 1335–1354.

Gunes, R., Aydin, M., Apalak, M.K., Reddy, J.N., 2011. The elasto-plastic impact analysis of functionally graded circular plates under low-velocities. Compos. Struct. 93, 860–869.

Huang, H., Chen, B., Han, Q., 2014. Investigation on buckling behaviors of elastoplastic functionally graded cylindrical shells subjected to torsional loads. Compos. Struct. 118, 234–240.

Javaheri, R., Eslami, M.R., 2012. Thermal Buckling of Functionally Graded Plates. AIAA J.

Jin, Z.H., Paulino, G.H., Dodds, R.H., 2003. Cohesive fracture modeling of elastic-plastic crack growth in functionally graded materials. Eng. Fract. Mech. 70, 1885–1912.

Lanhe, W., 2004. Thermal buckling of a simply supported moderately thick rectangular FGM plate. Compos. Struct. 64, 211–218.

Lee, Y.Y., Zhao, X., Reddy, J.N., 2010. Postbuckling analysis of functionally graded plates subject to compressive and thermal loads. Comput. Methods Appl. Mech. Eng. 199, 1645–1653.

Liew, K.M., Yang, J., Kitipornchai, S., 2003. Postbuckling of piezoelectric FGM plates subject to thermo-electro-mechanical loading. Int. J. Solids Struct. 40, 3869–3892.

Matsunaga, H., 2009. Thermal buckling of functionally graded plates according to a 2D higher-order deformation theory. Compos. Struct. 90, 76–86.

Mechanics, A., Office, P.S., 2007. Elastic-plastic buckling of infinitel y long plates resting on tensionless foundations.

Mori, T., Tanaka, K., 1973. Average stress in matrix and average elastic energy of materials with misfitting inclusions. Acta Metall. 21, 571–574.

Na, K.-S., Kim, J.-H., 2006. Thermal postbuckling investigations of functionally graded plates using 3-D finite element method. Finite Elem. Anal. Des. 42, 749–756.

Najafizadeh, M.M., Eslami, M.R., 2012. First-Order-Theory-Based Thermoelastic Stability of Functionally Graded Material Circular Plates. AIAA J.

Narayanan, R., Chow, F.Y., 1984. Ultimate capacity of uniaxially compressed perforated plates. Thin-Walled Struct. 2, 241–264.

Paik, J.K., 2005. Ultimate strength of dented steel plates under edge shear loads. Thin-Walled Struct. 43, 1475–1492.

Paley, M., Aboudi, J., 1991. Plastic buckling of metal matrix laminated plates. Int. J. Solids Struct. 28, 1139–1154.

Reddy, J.N., 2000. Analysis of functionally graded plates 684, 663–684.

Reddy, J.N., Chin, C.D., 1998. Thermomechanical Analysis of Functionally Graded Cylinders and Plates. J. Therm. Stress. 21, 593–626.

Samsam Shariat, B.A., Eslami, M.R., 2006. Thermal buckling of imperfect functionally graded plates. Int. J. Solids Struct. 43, 4082–4096.

Shakeri, M., Mirzaeifar, R., 2009. Static and Dynamic Analysis of Thick Functionally Graded Plates with Piezoelectric Layers Using Layerwise Finite Element Model. Mech. Adv. Mater. Struct. 16, 561–575.

Shanmugam, N.E., Thevendran, V., Tan, Y.H., 1999b. Design formula for axially compressed perforated plates. Thin-Walled Struct. 34, 1–20.

Sharma, K., Kumar, D., 2016a. Thermal postbuckling analysis of FGM plate with various shaped cutouts. Mech Adv Mater Struct 0, 0.

Sharma, K., Kumar, D., 2016b. Nonlinear stability and failure analysis of perforated FGM plate. INDIAN J. PURE Appl. Phys. 54, 665–675.

Shen, H.S., 2007. Thermal postbuckling behavior of shear deformable FGM plates with temperature-dependent properties. Int. J. Mech. Sci. 49, 466–478.

Shiota, I., Miyamoto, Y., 1997. Functionally graded materials 1996. Elsevier.

Singh, S.B., Kumar, A., 1999. Postbuckling response and strength of laminates under combined in-plane loads. Compos. Sci. Technol. 59, 727–736.

Soh, A.K., Bian, L.C., Chakrabarty, J., 2000. Elastic/plastic buckling of a composite flat plate subjected to uniform edge compression. Thin-Walled Struct. 38, 247–265.

Suresh, S., Mortensen, A., 1998. Fundamentals of Functionally Graded Materials: Processing and Thermomechanical Behaviour of Graded Metals and Metal-ceramic Composites. IOM Communications Limited.

Tamura, I., Tomato, Y., Ozawa, H., 1973. Strength and ductility of Fe-Ni-C alloys composed of austenite and martensite with various strength. Proc. third Conf. strength Met. Alloy. vol. 1. Cambridge Inst. Met. 1, 611–616.

Tohgo, K., Masunari, A., Yoshida, M., 2006. Two-phase composite model taking into account the matricity of microstructure and its application to functionally graded materials. Compos. Part A Appl. Sci. Manuf. 37, 1688–1695.

Touloukian, Y.S., Center, T.P.R., 1967. Thermophysical properties of high temperature solid materials. Vol. 1. Elements.-Pt. 1. Macmillan.

Williamson, R.L., Rabin, B.H., Byerly, G.E., 1995. FEM study of the effects of interlayers and creep in reducing residual stresses and strains in ceramic-metal joints. Compos. Eng. 5, 851–863.

Woo, J., Meguid, S. a., Stranart, J.C., Liew, K.M., 2005. Thermomechanical postbuckling analysis of moderately thick functionally graded plates and shallow shells. Int. J. Mech. Sci. 47, 1147–1171.

Wu, T.-L., Shukla, K.K., Huang, J.H., 2007. Post-buckling analysis of functionally graded rectangular plates. Compos. Struct. 81, 1–10.

Yaghoobi, H., Fereidoon, A., Khaksari Nouri, M., Mareishi, S., 2015. Thermal Buckling Analysis of Piezoelectric Functionally Graded Plates with Temperature-Dependent Properties. Mech. Adv. Mater. Struct. 22, 864–875.

Yamaki, N., 1960. Postbuckling behavior of rectangular plates with small initial curvature loaded in edge compression—(continued). J. Appl. Mech. 27, 335–342.

Yang, J., Shen, H., 2003a. Non-linear analysis of functionally graded plates under transverse and in-plane loads. Int. J. NonLinear Mech. 38, 467–482.

Yang, J., Shen, H.S., 2003b. Nonlinear bending analysis of shear deformable functionally graded plates subjected to thermo-mechanical loads under various boundary conditions. Compos. Part B Eng. 34, 103–115.

Zhang, Y., Huang, H., Han, Q., 2015. Buckling of elastoplastic functionally graded cylindrical shells under combined compression and pressure. Compos. Part B Eng. 69, 120–126.